CrystEngComm

ROYAL SOCIETY OF CHEMISTRY

PAPER

View Article Online
View Journal | View Issue

Cite this: *CrystEngComm*, 2025, **27**, 2470

Aldehyde-based triphenylethylene organic crystals for aniline vapour detection†

Elissa O. Shehayeb,[ad] Abdeljalil Assoud[b] and Vonika Ka-Man Au *[cd]

Received 7th January 2025,
Accepted 5th March 2025

DOI: 10.1039/d5ce00022j

rsc.li/crystengcomm

Air pollution, particularly from volatile organic compounds (VOCs), has been a major concern in the past century, especially with the increase in industrial activities. Aniline, one example of VOCs, is mainly involved in the manufacturing industry. Sensing the presence of aniline in prone locations is of great importance due to its hazardous environmental and health implications. This work presents the synthesis of fluorescent organic crystals of a novel compound, an aldehyde derivative of triphenylethylene, namely **TrPE-(CHO)$_3$**, which can visually portray the presence of aniline vapour by fluorescence quenching. Herein, we investigate the solid-state packing of **TrPE-(CHO)$_3$** in crystals and its properties, as well as the interactions occurring between the crystals and aniline, and thus elucidate the underlying reason for the selective sensing of aniline as compared to other VOCs. We also demonstrate a proof-of-concept display by coating a light-emitting diode with the synthesized material, which upon exposure to aniline, loses its cyan emission colour.

Introduction

Volatile organic compounds (VOCs) are a family of aromatic or aliphatic hydrocarbons with various functional groups, known for their ability to readily evaporate at ambient temperature and pressure.[1] VOCs are usually released into the atmosphere by natural or anthropogenic processes, posing alarming concerns due to their relative toxicity, mutagenicity, and carcinogenicity to humans and the environment.[2] One of the VOCs released into the environment from a variety of industries is aniline. Aniline is the simplest amino-substituted benzene that is usually synthesized by the catalytic hydrogenation of nitrobenzene, and it is a chemical feedstock that is extensively used in the manufacture of dyes, rubber, antioxidants, printer inks, explosives, and others.[3,4] The high toxicity of aniline, a classified class A VOC that can cause significant harm to the environment,[5] and has been proven to cause skin allergy, methemoglobinemia, oxidative and nitrosative stress, and even hemolysis,[4,6,7] has driven researchers to develop materials capable of selectively and efficiently monitoring its presence in the atmosphere. The recommended permissible occupational exposure limit to aniline vapour is 2 ppm according to the American Conference of Governmental Industrial Hygienists (ACGIH) and 5 ppm according to the Occupational Safety and Health Administration (OSHA).[8] Numerous studies published in the literature have focused on the sensing and/or capture of aniline vapour through different media including nanofibers,[9] gels,[10,11] thin films,[12] metal–organic frameworks (MOFs),[13,14] and so on.[15] Herein, however, we use chemically and thermally stable molecular structures that can selectively portray the presence of aniline vapour by fluorescence quenching.

Organic crystals are formed upon the orderly packing of molecular compounds *via* the interplay of inter- and intramolecular interactions to form a crystalline three-dimensional lattice.[16–18] Luminescent organic crystals are of great interest in applications such as luminescence turn on/off stimuli-responsive sensing,[19,20] microlasers,[21,22] and light-emitting diodes,[23,24] due to their practicality and ease of naked-eye visual differentiation. Achieving solid-state luminescence of organic compounds is usually a challenge due to the quenching or relatively weak emission of aggregates.[25,26] Hence, the aggregation-induced emission (AIE) phenomenon[27] of organic molecules is greatly desirable in the production of efficient electroluminescent materials. In particular, triphenylethylene derivatives are remarkable asymmetric AIE moieties formed of the central planar olefin core attached to three rotatable functionalized phenyl rings.[28]

In this paper, we report the synthesis of 4′,4‴,4⁗-(ethene-1,1,2-triyl)tris(([1,1′-biphenyl]-4-carbaldehyde)), herein called **TrPE-(CHO)$_3$**, a novel cyan-emitting aldehyde-functionalized triphenylethylene derivative. Its molecular structure, determined

[a] *Department of Chemistry, Burke Laboratory, Dartmouth College, Hanover, New Hampshire 03755, USA*
[b] *Department of Chemistry and the Waterloo Institute for Nanotechnology, University of Waterloo, Waterloo, Ontario, Canada*
[c] *Graduate School of Energy Science, Kyoto University, Yoshida-honmachi, Sakyo-ku, Kyoto 606-8501, Japan. E-mail: au@energy.kyoto-u.ac.jp*
[d] *Department of Science and Environmental Studies, The Education University of Hong Kong, 10 Lo Ping Road, Tai Po, New Territories, Hong Kong, P. R. China*
† Electronic supplementary information (ESI) available. CCDC 2405986. For ESI and crystallographic data in CIF or other electronic format see DOI: https://doi.org/10.1039/d5ce00022j

from single crystal X-ray diffraction, and its optical properties are reported. In addition, **TrPE-(CHO)$_3$** is proven to be efficient in the selective sensing of aniline vapour with respect to other VOCs, visually observed as turn-off fluorescence quenching of **TrPE-(CHO)$_3$** crystals. The interactions occurring between the synthesized molecule and aniline have been elucidated *via* a suite of spectroscopic and microscopic techniques.

Results and discussion

Synthesis and single crystal structure

In a similar approach to previously reported triphenylethylene derivatives,[25,26,28,29] **TrPE-(CHO)$_3$** is synthesized by a two-step procedure from commercially available starting materials, as schematized in Scheme S1.† Briefly, a Wittig–Horner reaction is performed by which the initial precursors are added consecutively to form the tribromo-intermediate **2** in a one-pot reaction, which is then purified by column chromatography. The purity of the intermediate is confirmed by ^{1}H- and ^{13}C-nuclear magnetic resonance (NMR) spectroscopy (Fig. S1 and S2†). This step is followed by a Pd-catalyzed Suzuki–Miyaura coupling reaction with 4-formylphenylboronic acid and potassium carbonate in tetrahydrofuran at 85 °C for the synthesis of **TrPE-(CHO)$_3$**. The final product is obtained in high yields after purification by column chromatography and is characterized by ^{1}H-NMR, ^{13}C-NMR, and mass spectrometry (low-resolution and high-resolution), whose results are presented in Fig. S3–S6.† The detailed synthetic procedure can be found in the ESI.† The slow evaporation of a 1 : 1 (v/v) ethyl acetate and hexane solvent mixture from the synthesized product, as described in the ESI,† afforded large crystals of the product suitable for single crystal X-ray diffraction. The single crystal structure of **TrPE-(CHO)$_3$** features a 3D asymmetric propeller formed of three twisted functionalized phenyl rings around a central double bond (Fig. 1a and S7†). These twists possess torsion angles of 26.47°, 31.65°, and 48.44°, mainly resulting from steric hindrance.[28] The 4-carbonyl phenyl rings attached to the *para*-positions of the three abovementioned phenyl rings are also twisted around the C–C bond connecting the two phenyl rings together with different angles of magnitude of around 30°. The latter twists can be a result of steric hindrance, as well as the forced packing effect of neighboring **TrPE-(CHO)$_3$** molecules through intermolecular interactions (Fig. 1b and c). These interactions include π–π interactions, observed as parallel displaced benzene ring structures with interplanar distances of around 3.5 Å (Fig. 1d), as well as π–π interactions between the benzene ring of one molecule and the conjugated C=O of another molecule with distances of 3.257 Å (Fig. 1e). Hydrogen-bonding between the aldehyde oxygen atom of one molecule and an aryl hydrogen atom of another molecule is observed with O···H distances of 2.714 Å, in addition to CH···π interactions between an aryl hydrogen atom of one molecule and a carbon atom of the benzene ring in another molecule with distances equal to 2.797 Å (Fig. 1e). Tables summarizing the crystal structure, coordinate positions of atoms, and the main values of distances, angles, and torsions can be found in Tables S2–S6.†

Characterization and optical properties of TrPE-(CHO)$_3$

The high crystallinity of packed **TrPE-(CHO)$_3$** molecules can be observed in its powder X-ray diffraction (PXRD) pattern in

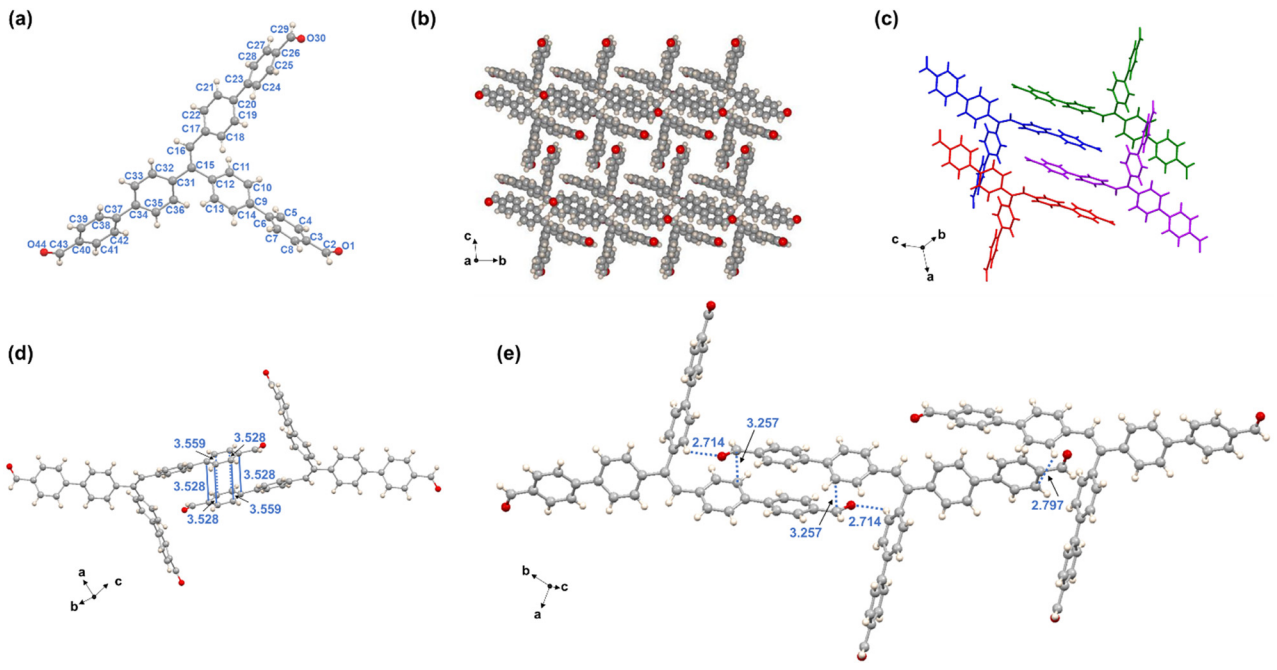

Fig. 1 (a) Labeled molecular structure of **TrPE-(CHO)$_3$**. (b) and (c) Packing of several molecules of **TrPE-(CHO)$_3$**. (d) Distances (Å) between the parallel displaced stacking of benzene rings from two different molecules of **TrPE-(CHO)$_3$**. (e) Short contact distances (Å) of the non-covalent interactions occurring between the different molecules of **TrPE-(CHO)$_3$**.

Fig. 2a. The main diffraction planes presented in the simulated diffraction pattern, which was extracted from the single crystal data, are strongly present in the PXRD trace of **TrPE-(CHO)$_3$**. We noted the appearance of some peaks (at around 2θ = 16° and 24°) with higher intensities in the experimental pattern compared to their respective peaks in the simulated pattern, which we have attributed to the preferred orientation of microcrystallites with respect to the X-ray diffraction source and detector.[30,31] In an effort to determine the apparent shape and optical properties of these crystals, they were observed under a polarized optical microscope (POM). Crystals of various sizes and shapes are observed with a birefringent nature, appearing as coloured crystals upon their alignment at a certain axis (Fig. 2b). This observation confirms the anisotropic domain of the studied crystals in their biaxial triclinic unit cells that allow double refraction of incident polarized light along one of its two optical axes.[32]

The optical properties of **TrPE-(CHO)$_3$**, mainly electronic absorption and emission, have been studied in different solvents at room temperature. In particular, the absorption spectra of **TrPE-(CHO)$_3$** in various solvents, as shown in Fig. S8,† are greatly similar to each other with minimal shifts. The main broad peak with a maximum wavelength of about 355 nm is comparable to other reported functionalized triphenylethylene derivatives, corresponding to π–π* transitions of the whole π-conjugated electron system.[26] Similarly, emission spectra at an excitation wavelength of 365 nm showed slight shifts in different solvents with a maximum wavelength of around 480 nm as depicted in Fig. S9.†

As triphenylethylene derivatives are known for their luminescence properties due to their extended π-conjugation, the emission properties of **TrPE-(CHO)$_3$** were studied. Upon photoexcitation at 365 nm, **TrPE-(CHO)$_3$** exhibits cyan emission in the solid state at room temperature, corresponding to a broad emission band with a peak at 480 nm, as shown in Fig. 2c. The CIE 1931 chromaticity coordinates of the colour emitted by **TrPE-(CHO)$_3$** are (0.163, 0.446), situated in the region combining different intensities of green and blue colours to obtain an overall cyan colour, as shown in Fig. 2d.

Selective aniline sensing

TrPE-(CHO)$_3$ exhibits fluorescence quenching upon its exposure to aniline vapour. In a setup, as illustrated in Fig. S10,† a small vial, filled half-way with aniline, is kept open and placed carefully in a larger vial containing **TrPE-(CHO)$_3$**, which is then capped tightly. The setup is kept at room temperature for 2 days to ensure saturation of the whole container with the aniline vapour. After 2 days, no emission from the solid is observed by the naked-eye upon the irradiation of UV-light at 365 nm (insets of Fig. 3a). The solid-state emission of **TrPE-(CHO)$_3$** is readily quenched upon its exposure to aniline vapour, as depicted in Fig. 3a. The selectivity of **TrPE-(CHO)$_3$** towards the sensing of aniline vapour is tested by repeating the experiment with vapours of other organic compounds. These include a variety of VOCs as well as primary,

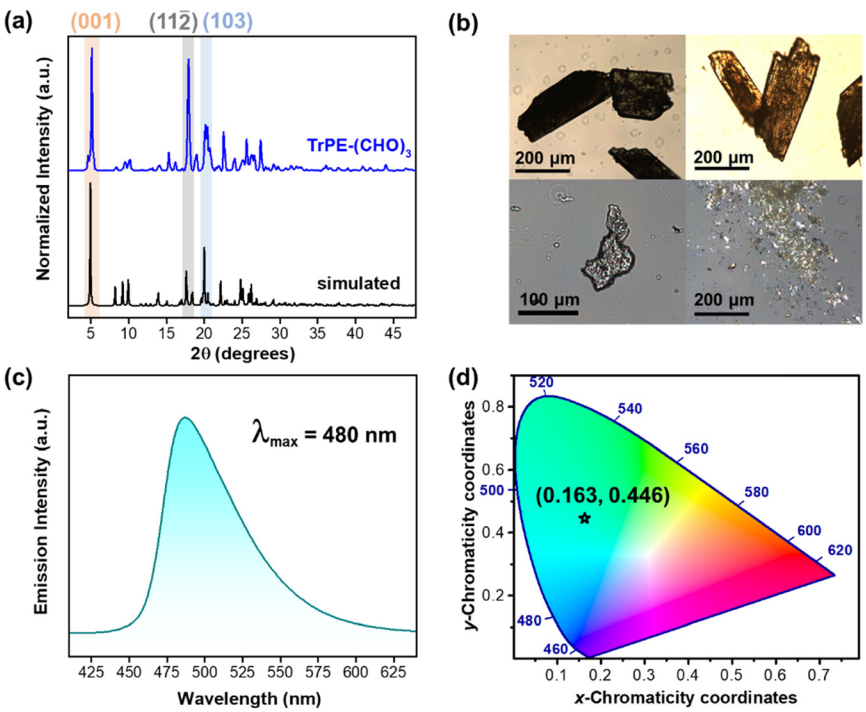

Fig. 2 (a) Experimental and simulated PXRD patterns of **TrPE-(CHO)$_3$**. (b) POM images of **TrPE-(CHO)$_3$** crystals at the assigned magnifications. (c) Solid-state emission spectrum of **TrPE-(CHO)$_3$** at room temperature, and (d) the corresponding CIE chromaticity diagram of **TrPE-(CHO)$_3$** at λ_{ex} = 365 nm.

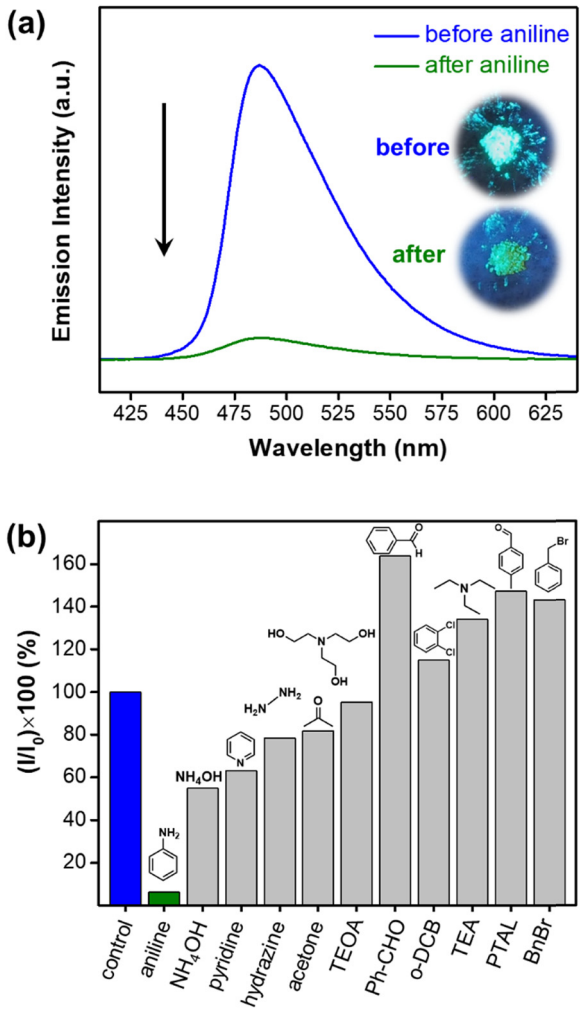

Fig. 3 (a) Emission spectra of **TrPE-(CHO)$_3$** before and after exposure to aniline vapour at λ_{ex} = 365 nm. Insets show photos of **TrPE-(CHO)$_3$**, under UV light irradiation of 365 nm, before and after its exposure to aniline. (b) Bar chart showing the change in fluorescence intensity of **TrPE-(CHO)$_3$** after exposure to different VOCs (NH_4OH = ammonium hydroxide; TEOA = triethanolamine; Ph–CHO = benzaldehyde; *o*-DCB = *o*-dichlorobenzene; TEA = triethylamine, PTAL = *p*-toluoyl aldehyde; BnBr = benzyl bromide).

secondary, and tertiary amines in an attempt to understand the mechanism of quenching. All setups are kept at room temperature, and the emission of the resulting solid is compared to a control sample which has been kept under ambient conditions. The results, as shown in Fig. 3b, reveal the selectivity of **TrPE-(CHO)$_3$** in sensing aniline vapour, in which complete turn-off of fluorescence is observed, whereas other VOCs give rise to either an increase or a slight decrease in luminescence. As shown in Table S1,† there is no direct correlation with the molecular diameters of the tested vapours nor with their respective boiling points, as their values were similar to those of aniline. Hence, we attribute the selectivity in this observation to the unique interactions occurring between the structures of **TrPE-(CHO)$_3$** and aniline.

Understanding the interactions between TrPE-(CHO)$_3$ and aniline

We hypothesized that there are two types of interactions, covalent and non-covalent interactions, occurring between the crystals and aniline. More specifically, we hypothesized that a Schiff-base reaction is taking place between the aldehyde functional groups on the surface of **TrPE-(CHO)$_3$** crystals and the amine groups of aniline molecules similar to observations previously reported in other studies.[33–35] This interaction greatly explains the fluorescence turn-off phenomenon described above, as the quenching of luminescence is attributed to photoinduced electron transfer occurring from the triphenylethylene chromophoric core to the imine linkage.[33,36] In addition, π–π interactions and hydrogen bonding are examples of non-covalent interactions that might be occurring between **TrPE-(CHO)$_3$** and aniline molecules.

In an effort to examine and prove the interaction occurring between **TrPE-(CHO)$_3$** and aniline, several experiments have been performed and compared before and after the subjection to aniline vapour. First, single crystals of **TrPE-(CHO)$_3$** have been exposed to aniline in a similar setup as described above. However, single crystal X-ray measurements of the **TrPE-(CHO)$_3$** exposed to aniline did not show any measurable diffractions, prohibiting analysis through this method. This observation, however, has increased our curiosity to understand how the initial crystalline structure is being disturbed upon the exposure to aniline vapour by utilizing additional techniques.

The PXRD patterns of **TrPE-(CHO)$_3$** after subjection to aniline show a shift in the initial diffraction peak at 2θ angles from 5.12° to 4.10°, as well as a substantial decrease in the peak intensities compared to the pristine crystals and the simulated pattern (Fig. 4a). The decrease in crystallinity has also been verified using scanning electron microscopy (SEM), by which we can see the differences in the sizes and shapes of **TrPE-(CHO)$_3$** crystals before and after their subjection to aniline vapour, as shown in Fig. 4b and S11.† In particular, at the same microscopy magnification, we have noticed how the original crystals with a homogeneous facet and a smooth surface break down to afford non-even surfaces with a rough texture, reconfirming the loss of crystallinity upon the interaction of **TrPE-(CHO)$_3$** with aniline. Taken together, the PXRD and SEM observations permit us to infer that a new phase of **TrPE-(CHO)$_3$** is generated upon its exposure to aniline. Particularly, we reasoned that this transformation occurs at the surface of the crystals as they are non-porous in nature (BET surface area = 7.8 ± 1.1 $m^2\ g^{-1}$, Fig. S12†), and their voids, depicted in Fig. S13,† are calculated to be 150.33 $Å^3$, equivalent to only 9.7% of the unit cell volume.

Energy dispersive X-ray (EDX) analysis, as shown in Fig. S14,† has confirmed the integration of nitrogen atoms, originating from the amino group of aniline, into the new crystals after aniline exposure, along with the presence of carbon and oxygen atoms, which are already present in the pristine **TrPE-(CHO)$_3$**. Upon computing the chemical composition of the crystals by EDX, the carbon and oxygen

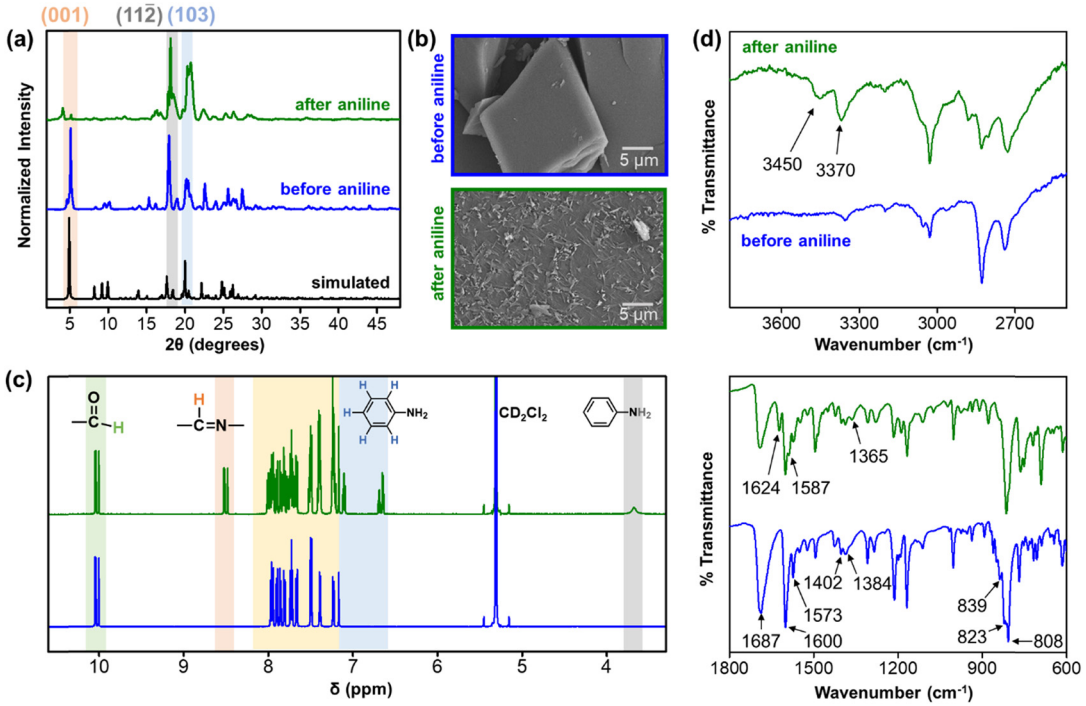

Fig. 4 Different experiments performed on **TrPE-(CHO)$_3$** crystals before (blue) and after (green) their exposure to aniline: (a) PXRD patterns, (b) SEM images, (c) ^{1}H-NMR spectra in CD_2Cl_2 at 500 MHz, and (d) zoomed-in FTIR spectra.

atomic percentages decrease from 87.82% and 12.18% to 85.51% and 8.57% before and after aniline exposure, respectively. These decreases are accommodated by the presence of nitrogen atoms after aniline exposure with an atomic composition of 5.92%.

The nature of the bonds occurring between these atoms is assessed by X-ray photoelectron spectroscopy (XPS). The presence of carbon (C 1s) in the binding energy range between 280 and 290 eV and of oxygen (O 1s) between 524 and 536 eV is obvious in both recorded spectra before and after aniline exposure.[37] However, an extra peak at a binding energy of around 400 eV is observed in the survey spectrum after the subjection to aniline vapour, which refers to the extra nitrogen atoms (N 1s) present in the resulting sample (Fig. S15†).[38] High-resolution spectra recorded at these specific binding energies are shown in Fig. S16,† in addition to the deconvolution of the N 1s band showing the presence of imine and amine type linkages in **TrPE-(CHO)$_3$** upon aniline exposure.

In order to gain an insight into the chemical structure of **TrPE-(CHO)$_3$** after aniline exposure, ^{1}H- and ^{13}C-NMR spectra of the solid obtained are collected and compared to those of the pristine crystals. Fig. 4c highlights the main differences in the ^{1}H-NMR spectra and Fig. S17† shows magnifications of these spectra at the peaks of interest. Upon critical examination of the spectra, we noticed that the original peaks of **TrPE-(CHO)$_3$** are still present, even after aniline exposure, particularly those pertaining to the unsymmetrical aldehyde protons at chemical shifts δ = 10.02, 10.06, and 10.07 ppm. However, new peaks at δ = 8.51, 8.54, and 8.55 ppm are observed and are attributed to protons attached to the carbon atoms of Schiff-base imine linkages, resulting from the chemical reaction of the aldehyde functional groups of **TrPE-(CHO)$_3$** and the amine functional groups of aniline. In addition, we noticed the presence of significant multiplets at δ = 6.5–6.6 and 7.0–7.1 ppm and a broad band at δ = 3.7 ppm pertaining to the aromatic protons and the amino group protons of aniline, respectively. These observations allow us to conclude that the aldehyde functional groups of some molecules of **TrPE-(CHO)$_3$** chemically reacted with aniline, whereas others did not, further confirming our hypothesis of the presence of two types of interactions occurring. The loss of symmetry resulting from the newly formed molecules and their overlap with the peaks of pristine **TrPE-(CHO)$_3$** is reflected in the overlap of several peaks at the aromatic region with chemical shifts ranging between 7.2 and 8.0 ppm, which are difficult to be assigned to particular protons. This loss of symmetry is also highlighted in the extra aromatic peaks appearing in the ^{13}C-NMR spectrum after aniline exposure when compared to that of **TrPE-(CHO)$_3$** (Fig. S18†). The proposed structures of the expected compound(s) are provided in Fig. S19,† in addition to a schematic diagram depicting the possible non-covalent interactions occurring between **TrPE-(CHO)$_3$** and aniline (Fig. S20†). These various interactions are not only able to distort the crystal packing of **TrPE-(CHO)$_3$** resulting in the loss of its crystallinity but are also capable of quenching its fluorescence. We believe that this variety in interactions is unique to aniline, which possesses a π-surface and a nitrogen atom at an appropriate

geometry for interacting with **TrPE-(CHO)$_3$** (Fig. S20†), and thus causes the selective sensing response towards it rather than the other tested amines.

Fourier transform-infrared (FT-IR) spectra for **TrPE-(CHO)$_3$** samples before and after aniline exposure were obtained and compared in Fig. 4d and S21.† Similar to the NMR findings, all peaks pertaining to **TrPE-(CHO)$_3$** persist after its exposure to aniline in addition to the presence of newly-appeared peaks. The significant FT-IR peaks of pristine **TrPE-(CHO)$_3$** and their corresponding assignments are listed as follows: ν = 1687 cm^{-1} for the aromatic carbonyl (C═O) stretching, 1600 and 1573 cm^{-1} for conjugated aromatic C═C stretching, 1402 and 1384 cm^{-1} for aldehyde C–H bending, 839 cm^{-1} for trisubstituted C═C bending, and 808 cm^{-1} for 1,4-disubstituted benzene derivative C–H bending vibrations. The additional peaks observed after aniline exposure are primarily at ν = 3450 and 3370 cm^{-1} attributed to N–H stretching vibrations of aniline, at ν = 1623 and 1587 cm^{-1} corresponding to N–H bending vibrations of aniline or C═N stretching vibrations of the imine linkage, and at ν = 1365 cm^{-1} pertaining to aromatic C–N stretching vibrations.

LED application

To evaluate the potential of utilizing **TrPE-(CHO)$_3$** in practical applications, the heat stability of the compound has been studied by thermogravimetric analysis (TGA). **TrPE-(CHO)$_3$** possesses high thermal stability to temperatures above 400 °C, which is comparable to other previously synthesized triphenylethylene derivatives.[26] The TGA plot shown in Fig. S22† suggests that **TrPE-(CHO)$_3$** starts to decompose at 418 °C. Comparing the TGA plot of pristine **TrPE-(CHO)$_3$** to that after its subjection to aniline vapour, we notice an initial weight loss of around 9% across the 60–185 °C temperature range for the latter plot, which we attribute to the loss of aniline molecules physically adsorbed onto the surface of the **TrPE-(CHO)$_3$** structure, particularly since the boiling point of aniline is 184 °C.[8]

As a proof of concept, a 365 nm UV LED chip that functions at 3 V was coated with **TrPE-(CHO)$_3$**. The cover of the LED chip was removed, and the coated chip was placed in a closed vial with aniline vapour, similar to the setup followed for the sensing of aniline with **TrPE-(CHO)$_3$** in the solid state. Fig. 5 shows photos of the LED before and after its exposure to aniline vapour. It can be observed that the luminescence of the coated LED is completely quenched in the presence of aniline, and the LED chip no longer illuminates.

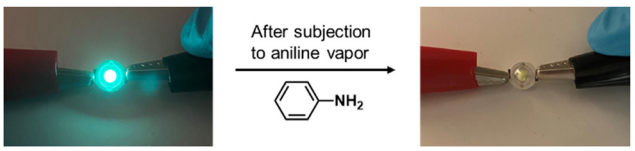

Fig. 5 Photos of the TrPE-(CHO)$_3$-coated LED chip before and after its exposure to aniline while turned on in both cases.

Conclusions

In summary, we have reported the synthesis and characterization of a novel organic compound, **TrPE-(CHO)$_3$**, in addition to its single crystal structure. We have demonstrated that the crystals can visually portray the presence of aniline selectively by their fluorescence quenching when exposed to aniline vapour as compared to other VOCs. As proven by different spectroscopic techniques, the quenching of fluorescence is assumed to be due to a combination of chemical and physical interactions occurring between the aldehyde groups and the extended aromatic π-system of **TrPE-(CHO)$_3$** with the structure of aniline. We have also shown the practical applicability of this material *via* the fabrication of a coated LED, by which the fluorescence quenching is easily visible, further highlighting the usability of these luminescent organic crystals in environmental sensing.

Data availability

The data supporting this article have been included as part of the ESI.† Crystallographic data for **TrPE-(CHO)$_3$** have been deposited at the joint Cambridge Crystallographic Data Centre and Fachinformationszentrum Karlsruhe Access Structures service under deposition number CCDC 2405986.

Author contributions

Elissa O. Shehayeb: conceptualization, writing – original draft, investigation and formal analysis (lead: all experiments). Abdeljalil Assoud: investigation and formal analysis (supporting: determination of the single crystal structure). Vonika Ka-Man Au: conceptualization, writing – review & editing, formal analysis, supervision, funding acquisition.

Conflicts of interest

There are no conflicts to declare.

Acknowledgements

V. K.-M. A. acknowledges a start-up research fund from Kyoto University. This work was partially supported by the Early Career Scheme from the Research Grants Council of the Hong Kong Special Administrative Region, P. R. China (EdUHK 28300220).

Notes and references

1 R. Montero-Montoya, R. López-Vargas and O. Arellano-Aguilar, *Ann. Glob. Health*, 2018, **84**, 225–238.
2 A. J. Li, V. K. Pal and K. Kannan, *J. Environ. Chem. Ecotoxicol.*, 2021, **3**, 91–116.
3 National Research Council, *Acute Exposure Guideline Levels for Selected Airborne Chemicals: Volume 1*, The National Academies Press, Washington, DC, 2000.
4 Y. Wang, H. Gao, X.-L. Na, S.-Y. Dong, H.-W. Dong, J. Yu, L. Jia and Y.-H. Wu, *Int. J. Environ. Res. Public Health*, 2016, **13**, 1188.

5 I. Marlowe, C. Bone and S. Byfield, *The categorisation of volatile organic compounds*, Her Majesty's Inspectorate of Pollution, Great Britain, 1995.
6 J. Pauluhn, *Toxicol. Sci.*, 2004, **81**, 198–215.
7 N. Hudson and G. S. Dotson, NIOSH skin notation (SK) profile: Aniline [CAS No. 62-53-3], 2015.
8 J. A. Young, *J. Chem. Educ.*, 2009, **86**, 683.
9 Y. Che and L. Zang, *Chem. Commun.*, 2009, 5106–5108.
10 L. Wang, B. Wang and J. Song, *RSC Adv.*, 2022, **12**, 23169–23175.
11 H. Su, R. Liu, M. Shu, M. Tang, J. Wang and H. Zhu, *Dyes Pigm.*, 2019, **162**, 52–58.
12 H. Che, S. Yan, Y. Nie, X. Tian and Y. Li, *J. Hazard. Mater.*, 2022, **435**, 129016.
13 F.-P. Yang, Q.-T. He, H. Jiang, Z. Li, W. Chen, R.-L. Chen, X.-Y. Tang, Y.-P. Cai and X.-J. Hong, *Inorg. Chem.*, 2022, **61**, 10844–10851.
14 H. Wang, W. P. Lustig and J. Li, *Chem. Soc. Rev.*, 2018, **47**, 4729–4756.
15 L. Wang and J. Song, *Sens. Actuators, A*, 2023, **362**, 114676.
16 D. P. Karothu, J. Mahmoud Halabi, E. Ahmed, R. Ferreira, P. R. Spackman, M. A. Spackman and P. Naumov, *Angew. Chem., Int. Ed.*, 2022, **61**, e202113988.
17 A. Nangia, *Acc. Chem. Res.*, 2008, **41**, 595–604.
18 J. D. Dunitz and A. Gavezzotti, *Angew. Chem., Int. Ed.*, 2005, **44**, 1766–1787.
19 Y. Sagara, K. Takahashi, T. Nakamura and N. Tamaoki, *J. Mater. Chem. C*, 2020, **8**, 10039–10046.
20 Q. Chen, X. Chen, M. Liang, Y. Han and P. Xue, *CrystEngComm*, 2022, **24**, 2575–2590.
21 W. Zhang, J. Yao and Y. S. Zhao, *Acc. Chem. Res.*, 2016, **49**, 1691–1700.
22 J. Liang, Y. Yan and Y. S. Zhao, *Acc. Mater. Res.*, 2021, **2**, 340–351.
23 X. Yang, X. Feng, J. Xin, P. Zhang, H. Wang and D. Yan, *J. Mater. Chem. C*, 2018, **6**, 8879–8884.
24 E. O. Shehayeb and V. K.-M. Au, *ACS Appl. Nano Mater.*, 2024, **7**, 18655–18675.
25 B. Xu, Z. Chi, Z. Yang, J. Chen, S. Deng, H. Li, X. Li, Y. Zhang, N. Xu and J. Xu, *J. Mater. Chem.*, 2010, **20**, 4135–4141.
26 X.-F. Li, Z.-G. Chi, B.-J. Xu, H.-Y. Li, X.-Q. Zhang, W. Zhou, Y. Zhang, S.-W. Liu and J.-R. Xu, *J. Fluoresc.*, 2011, **21**, 1969–1977.
27 J. Mei, N. L. Leung, R. T. Kwok, J. W. Lam and B. Z. Tang, *Chem. Rev.*, 2015, **115**, 11718–11940.
28 J. Chen, J. Xia, H.-J. Yu, J.-X. Zhong, X.-K. Wu, Y.-S. Qin, C. Jia, Z. She, D.-B. Kuang and G. Shao, *Chem. Mater.*, 2019, **31**, 5431–5441.
29 X. Zhang, H. Sun, K.-H. Low, T. Yu and V. K.-M. Au, *Mater. Chem. Front.*, 2023, **7**, 3332–3339.
30 C. F. Holder and R. E. Schaak, *ACS Nano*, 2019, **13**, 7359–7365.
31 R. A. Mayo, K. M. Marczenko and E. R. Johnson, *Chem. Sci.*, 2023, **14**, 4777–4785.
32 M. Xia, M. Mutailipu, F. Li, Z. Yang and S. Pan, *Cryst. Growth Des.*, 2021, **21**, 1869–1877.
33 Y. Fu, Y. Gao, L. Chen, Q. He, D. Zhu, H. Cao and J. Cheng, *RSC Adv.*, 2014, **4**, 46631–46634.
34 J. Hu, R. Liu, S. Zhai, Y. Wu, H. Zhang, H. Cheng and H. Zhu, *J. Mater. Chem. C*, 2017, **5**, 11781–11789.
35 Z. Jiao, Y. Zhang, W. Xu, X. Zhang, H. Jiang, P. Wu, Y. Fu, Q. He, H. Cao and J. Cheng, *ACS Sens.*, 2017, **2**, 687–694.
36 H. Ding, J. Li, G. Xie, G. Lin, R. Chen, Z. Peng, C. Yang, B. Wang, J. Sun and C. Wang, *Nat. Commun.*, 2018, **9**, 5234.
37 M. H. Engelhard, T. C. Droubay and Y. Du, X-ray Photoelectron Spectroscopy Applications, in *Encyclopedia of Spectroscopy and Spectrometry*, ed. J. C. Lindon, G. E. Tranter and D. W. Koppenaal, Elsevier, 3rd edn, 2017, pp. 716–724.
38 M. Kehrer, J. Duchoslav, A. Hinterreiter, M. Cobet, A. Mehic, T. Stehrer and D. Stifter, *Plasma Processes Polym.*, 2019, **16**, 1800160.

